

The Submillimeter Array Polarimeter

Daniel P. Marrone^{a,b}, Ramprasad Rao^c

^aJansky Fellow, National Radio Astronomy Observatory, USA

^bUniversity of Chicago, KICP, Chicago, IL, USA

^cSMA Project, Academia Sinica Institute of Astronomy & Astrophysics, Taipei, Taiwan

ABSTRACT

We describe the Submillimeter Array (SMA) Polarimeter, a polarization converter and feed multiplexer installed on the SMA. The polarimeter uses narrow-band quarter-wave plates to generate circular polarization sensitivity from the linearly-polarized SMA feeds. The wave plates are mounted in rotation stages under computer control so that the polarization handedness of each antenna is rapidly selectable. Positioning of the wave plates is found to be highly repeatable, better than 0.2 degrees. Although only a single polarization is detected at any time, all four cross correlations of left- and right-circular polarization are efficiently sampled on each baseline through coordinated switching of the antenna polarizations in Walsh function patterns. The initial set of anti-reflection coated quartz and sapphire wave plates allows polarimetry near 345 GHz; these plates have been used in observations between 325 and 350 GHz. The frequency-dependent cross-polarization of each antenna, largely due to the variation with frequency of the retardation phase of the single-element wave plates, can be measured precisely through observations of bright point sources. Such measurements indicate that the cross-polarization of each antenna is a few percent or smaller and stable, consistent with the expected frequency dependence and very small alignment errors. The polarimeter is now available for general use as a facility instrument of the SMA.

Keywords: Polarization, Submillimeter, Interferometry

1. INTRODUCTION

As the first dedicated submillimeter interferometer, the Submillimeter Array (SMA) provides unique capabilities for detailed study of the dusty sites of star formation. In particular, measurements of polarized dust emission, which traces the structure of the magnetic field in the plane of the sky (B_{\perp}), benefit greatly from higher frequencies and finer angular resolution. The flux density from optically thin warm dust emission rises like ν^{3-4} , multiplying the emission by factors of several between the 230 GHz band of millimeter interferometers such as PdBI and CARMA and the 345 GHz band of the SMA. Furthermore, structure is expected in the magnetic field on scales as small as ~ 100 AU in star forming regions, corresponding to $\sim 1''$ in even the nearest objects. Previous observations of polarized dust emission have generally been made at lower frequency and few arcsecond resolution or higher frequencies with no better than $10''$ resolution. The SMA provides the first opportunity to examine polarization at both high frequencies and high angular resolution. Illuminating the important and poorly understood role of the magnetic field in the star formation process provides a strong motivation for adding a polarimetric capability to the SMA. In addition, there are other targets, such as the polarization signatures of low-luminosity accretion,¹ that are accessible only near submillimeter frequencies.

The SMA was designed to allow polarimetry, but requires additional hardware to enable these observations. Most importantly, the SMA can measure only a single linear polarization at a given frequency, although this will change for some receivers in future upgrades. Therefore, modulation of the polarization sensitivity of each antenna is required in order to recover complete polarization information. Moreover, the interferometric measurement of linear polarization is best made with circularly-polarized receivers (see, e.g., ref. 2), so a linear-to-circular polarization conversion is desirable. The instrument described here provides the polarization conversion and rapid modulation that is required for these observations. We outline the instrument design, control system, calibration procedures and results, and provide examples of the science enabled by the polarimeter.

Further author information: (Send correspondence to D.P.M.)

D.P.M.: E-mail: dmarrone@oddjob.uchicago.edu, Telephone: 1 773 834 9785

R.R.: E-mail: rrao@sma.hawaii.edu, Telephone: 1 808 961 2935

2. POLARIMETER INSTRUMENT

2.1 Telescope Optics

The Submillimeter Array is composed of eight 6-meter diameter antennas on alt-az mounts. In these Cassegrain telescopes the receivers are mounted in a fixed cryostat at a Nasmyth focus. The relay optics between the secondary mirror and the cryostat consist of four mirrors*; two of these are curved and serve, with the lenses that are specific to each receiver band, to image the receiver feedhorn apertures onto the secondary mirror. The optics also generate an intermediate image of the feeds at an accessible location between the curved mirrors that is intended to accommodate calibration loads and polarizing elements. The polarimeter hardware is designed for installation at this location for polarimetric observations and easy removal to return to normal SMA operation.

2.2 Quarter-wave Plates

The linear-to-circular polarization conversion that is central to polarimetry with the SMA is achieved with a quarter-wave plate (QWP). A QWP is an anisotropic optical element that introduces a delay of one quarter wavelength between orthogonal linear polarizations. When the QWP axes are oriented at 45° to incident linear polarization, the polarization component along the “slow” axis of the wave plate is delayed and pure circular polarization is produced. By rotating the QWP by 90° the handedness of the circular polarization can be reversed.

Wave plates are ubiquitous in polarimetric experiments. Half-wave plates rotate linear polarization and are often used to modulate the polarization sensitivity of a detector of fixed polarization. Examples include the polarimeters for the submillimeter cameras on the JCMT³ and CSO,⁴ and various CMB polarization experiments.^{5,6} Quarter-wave plates have also been employed to generate circular polarization for interferometers with linear feeds, including the Berkeley-Illinois-Maryland Array⁷ and the Owens Valley Radio Observatory millimeter array.⁸

In the simplest design, half- or quarter-wave plates are single elements of birefringent material tuned in thickness to provide the appropriate path delay. However, this difference in propagation distance provides the desired phase delay at just one frequency, with a phase error that increases linearly away from this frequency. More complicated designs incorporating multiple elements can provide a nearly fixed phase delay over a large bandwidth.^{9,10} These designs are less frequently used but may become common as a result of the bandwidth requirements of bolometer-based CMB polarization experiments.¹¹ In the case of the SMA, such a broadband design could allow polarimetry across the full RF bandwidth of a given receiver band, or possibly all bands at once for very complicated designs.¹² Nevertheless, SMA science goals do not justify the added complication and loss of these designs, as there are few spectral lines that are interesting for polarimetry at SMA sensitivity and little to be gained by continuum polarimetry at two frequencies within a single receiver band. Instead, the 345 GHz QWPs of the SMA polarimeter use the single-element design, designed for an optimal frequency near the $J = 3 \rightarrow 2$ line of CO (345.8 GHz). This nearly bisects the most interesting frequency range in this band, between the atmospheric cutoff near 360 GHz and the masing¹³ water line at 325 GHz, minimizing the retardation error at both ends of the range.

Wave plates can be made from materials with natural or manufactured birefringence. The SMA wave plates are made from low-loss naturally anisotropic crystals, either quartz or sapphire (Table 1). To minimize reflections from the QWPs, which degrade the receiver sensitivity and can generate standing waves in the optical path, anti-reflection (AR) coatings have been applied. The ideal (monochromatic) AR coating is a quarter-wave thick with an index of refraction that is the geometric mean of the indices of the materials on either side of it. For quartz in air this is roughly 1.46, which is fairly close to the index of low-density polyethylene (LDPE), $n_{LDPE} = 1.514$.¹⁴ The larger index of sapphire is not particularly well matched by common polymer materials and for simplicity was also coated with LDPE. The expected reflectivity of the sapphire plates over the range of operating frequencies is 0–7%, much larger than the expected $< 1\%$ absorption in the sapphire. Measurements of the quartz wave plates near the optimum frequency indicate that they are 98% transmissive, resulting in a 9% increase in the system temperature under typical operating conditions.

*The optical system is described in the SMA Project Book, http://sma-www.cfa.harvard.edu/private/eng_pool/table.html

Table 1. Properties of the 345 GHz quarter-wave plates of the SMA polarimeter.

	Quartz Plates	Sapphire Plates
Quantity	7	1
Material	X-cut quartz	A-cut Hemlux sapphire
Indices of Refraction		
Ordinary	2.106^{15}	3.064^{16}
Extraordinary	2.154^{15}	3.404^{16}
Thickness (mm)	4.566 ± 0.003	0.640
Central Frequency (GHz)		
Nominal	342.0	345.5
Measured	347.7 ± 1.5	339.5
Anti-Reflection Coating		
Material	LDPE	LDPE
Mean Thickness (μm)	140–160	133
Peak-to-Peak Variation (μm)	3–14	10

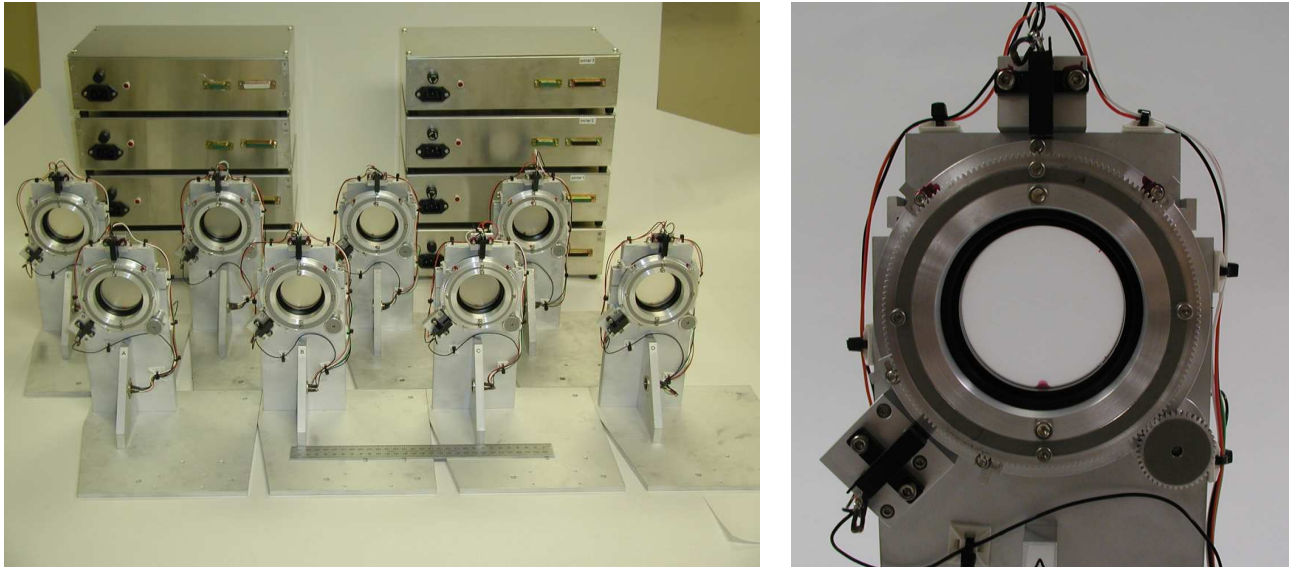


Figure 1. *Left*: The wave plate positioners and control computers of the SMA polarimeter. *Right*: Closeup of the rotation stage and QWP. Optical brakes are visible at the top and the bottom left. The adjustable flags that determine the wave plate positions are visible on the circumference of the rotation stage at $\pm 45^\circ$ from the optical brake at the top and at $\pm 22.5^\circ$ from the brake at the bottom left.

2.3 Positioning Hardware

In order to convert the SMA to circular polarization sensitivity the QWPs must be repeatably aligned to the feed polarization and be rotatable to select LCP or RCP. This is achieved with a computer-controlled mount and rotation system, the wave plate positioning hardware (Fig. 1). The QWPs are held in a rotation stage driven by a gear and DC motor. There is no encoder to monitor the position of the motor or rotation stage, rather, the wave plate positions are determined by two optical brakes (opto-interrupters) and four adjustable positioning flags on the circumference of the rotation stage (Fig. 1, right). These flags determine four angular positions for the wave plate, two of which set the $\pm 45^\circ$ position angles that convert the feed polarization to left- and right-circular polarization. The other two flags are monitored by a second optical brake and could be used to set positions $\pm 22.5^\circ$, allowing half-wave plates to switch a feed between two linear polarizations 90° apart.

Stability of the polarization properties of the SMA requires precisely repeatable positioning of the QWPs.

Any unnoticed error in positioning, such as that due to backlash or lost encoder counts, would introduce a change in the instrumental polarization and corrupt the calibration. We have used optical brakes because they are immune to backlash in the motor and do not rely on repeated contact, as a hard stop would. To accurately recover the intended stopping point for each orientation the edge of the positioning flag is found via a two-step process. The coarse alignment is derived from a slew at the maximum motor speed that ends when the flag interrupts the beam. Due to differences in the friction between wave plate mounts, the position determined in this way can be inaccurate by a degree or more and might be expected to change with temperature as the pressure on the bearing changes. Much greater accuracy is obtained in the second step, where the motor makes rapid pulsed movements until the correct edge of the flag (depending on the initial and final positions) is driven out of the opto-interrupter beam. Measurements of the positional repeatability achieved through this procedure found it to be better than the measurement precision, around 0.2° , which is more than adequate given the astronomical calibration limitations.

The wave plate positioning hardware operates and interfaces with the rest of the array through dedicated control computers. Each wave plate mount is controlled by a compact (PC-104 form-factor) disk-less computer that is accessed via a remote procedure call (RPC) application. The RPC server controls the plate movements, reports failures in acquiring positions, and can re-initialize the rotation stage to re-establish the location should it be lost.

The SMA QWPs must switch rapidly between the left- and right-circular polarization states to limit the observing time lost to switching. The motor and gear ratio have been chosen to ensure that the switch between the widely separated LCP and RCP positions can be achieved in less than 2 seconds in either direction. Upon initial deployment the positioners were found to switch in 1.5–1.9 seconds. Four years later the switching time has degraded very little, to 1.6–2.0 seconds in a recent measurement.

2.4 Polarimetric Observations

At present, most SMA antennas have only a single 345 GHz feed and therefore cannot sample both polarizations at the same frequency simultaneously. To recover the full polarization information we use the wave plates to switch the antennas between LCP and RCP in a coordinated temporal sequence. The switching patterns of the antennas are described by orthogonal two-state sequences known as Walsh functions. Well-chosen patterns will sample all four polarization combinations four times each on every baseline in a 16-step cycle. Averaging the visibilities over the cycle time results in quasi-simultaneous measurements of all polarizations. Under typical observing conditions this cycle is completed in 4–6 minutes.

The polarization switching results in significantly poorer sensitivity than that achieved in normal SMA observations. A significant portion of the degradation is caused by the time lost to switching polarization states and the process of stopping and restarting the correlator. For the 15-second integrations normally used, an additional 5 seconds per integration are lost to this overhead. Longer integrations would reduce the fractional impact of the overhead but risk decoherence when averaging over the polarization cycle. The most important cause of sensitivity loss is the time-multiplexing of the polarization sensitivity. On any baseline only half of the integrations in the polarization switching cycle are sensitive to Stokes I (LL and RR correlations) and half sensitive to Stokes Q and U (the linear polarization, LR and RL correlations). Combining these two effects, the integration time for the total intensity or linear polarization is approximately $3/8$ of that for normal SMA observations. Furthermore, the QWPs raise system temperature by $\sim 10\%$, as discussed above, for a total increase in the rms noise of approximately $1.8\times$.

3. CALIBRATION

3.1 Instrumental Polarization

Proper determination of the polarization of an astronomical source requires calibration of the instrumental polarization. The response of the SMA antennas, including the feeds and wave plates, can be modeled by a term representing the sensitivity to the desired polarization plus a fractional sensitivity to the orthogonal polarization, a complex “leakage” term.² To lowest order, the leakage mixes the total intensity (Stokes I) with the linear polarization (Q and U). For typical submillimeter sources the astronomical linear polarization is no

more than ten percent, while the leakage terms are often of similar magnitude, so these contributions must be removed precisely in order to determine the polarization of the target source. Fortunately, the instrumental and astronomical polarizations are separable for alt-azimuth mounted telescopes and sources of known polarization structure. Telescopes with non-equatorial mounts, such as the SMA antennas, see an apparent rotation of the target source as it moves across the sky, which distinguishes source and antenna polarization. Therefore, observations of a bright point source over a large range of parallactic angles allow determination of the leakages and are included in most SMA polarimetry tracks. The frequency coverage of the leakage measurements has been determined by the science goals of the polarimetric projects, resulting in very redundant data at few frequencies. This type of sampling provides very good measurements of stability and reproducibility in the leakage determinations, as described below. The spectral properties of the leakages are more poorly determined, but can also be examined from these data (Sec. 3.3).

3.2 Stability and Measurement Precision

Fig. 2 shows the real and imaginary components of the leakages measured for each antenna at four frequencies that have been repeated several times (two array tunings with two sidebands 10 GHz apart for each tuning). The leakages were measured over a period of a few months in 2005 and 2006, allowing investigation of the repeatability of the measurement and the stability of the system. Measurements at the same frequency and for the same polarization state (leakage of RCP into LCP, d_R , or LCP into RCP, d_L) form tight groups, even between years. The leakages appear to be as stable on long (one year) timescales as they are across periods of weeks. The spread in values in the $\text{Re}[d]$ direction is due to the linear variation of the QWP retardation with frequency, this is discussed further below.

Taking all of the measurements together, the average scatter in the leakage measurements is 0.4%. For most of these measurements, made at a time when the calibration source (3C454.3) was undergoing a large flare and was exceptionally bright, the measurement uncertainty was 0.1–0.15%, smaller than the scatter. If the scatter represents a random variation in the leakages that is uncorrelated between antennas, the expected false polarization signal introduced into an snapshot polarization observation would be 0.15%. In a long synthesis this is further reduced by the parallactic angle rotation of the source polarization. In the other extreme, if the leakage changes in any given observation are fully correlated in a way that directly converts I to Q or U , as much as the full leakage error may be introduced into a snapshot polarization measurement. Just as in the case of random errors, parallactic angle rotation will reduce the average polarization error across the whole track. However, there are few systematic errors that should operate to introduce correlated leakage errors and these data do not show such correlation, so this worst case is unlikely to be realized.

3.3 Frequency Dependence

To first order the leakage (d) depends on the frequency offset ($\delta = [\nu - \nu_0]/\nu_0$), orientation error (θ), and difference in the field reflection coefficient along the two QWP axes (ϵ) as¹⁷

$$d \simeq -\frac{\pi\delta(\nu)}{4} + \left(-\theta + \frac{\epsilon(\nu)}{2}\right)i. \quad (1)$$

Fitting the variation of the real component of the leakage with frequency, visible in Fig. 2 provides a determination of the optimum frequency of the plates. For the seven quartz plates this is 347.7 GHz with a scatter of 1.5 GHz, while the sapphire plate is tuned to 339.5 GHz. Differences between the nominal and observed central frequencies are largely due to the uncertainty in the literature values for the birefringence ($n_e - n_o$) of the QWP materials (10% for quartz). The slope of the variation with frequency should also be inversely proportional to the optimum frequency; the value of ν_0 derived in this way is poorly constrained but agrees with the intercept results. The imaginary components provide a measure of the alignment error in the absence of the ϵ term, but unfortunately the scatter in coating thickness ensures that there is non-negligible reflectivity in some of the plates. From other techniques, the alignment errors are found to be 0.3° or less.

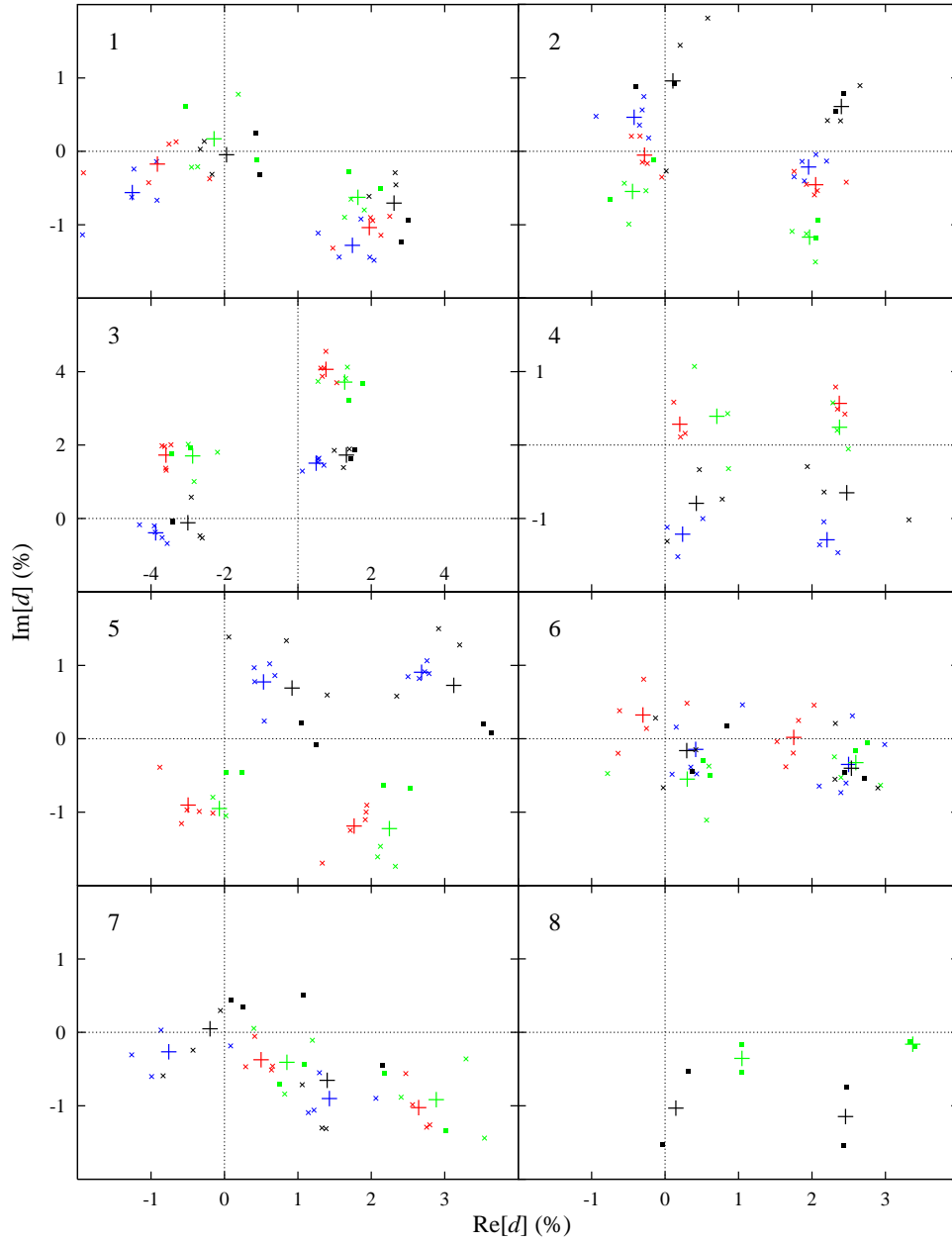


Figure 2. Leakages measured in 2005 and 2006. Each plot represents a single antenna, identified at the upper left. Leakages are plotted in the complex plane, with with equal linear scales in the real and imaginary axes. The red and blue points represent d_R and d_L , respectively, at 338.0 GHz (points at right in each plot) and 348.0 GHz (points at left). Green and black points represent d_R and d_L , respectively, at 336.5 GHz (right) and 346.5 GHz (left). The mean value of d_R (d_L) for each frequency is represented by a large red/green (blue/black) +. Individual measurements from 2005 (\times) and 2006 (\blacksquare) are marked with smaller symbols. The subplot for antenna 3, which hosted the sapphire plate, has a linear scale twice as large as those for the other antennas, as shown by its labels.

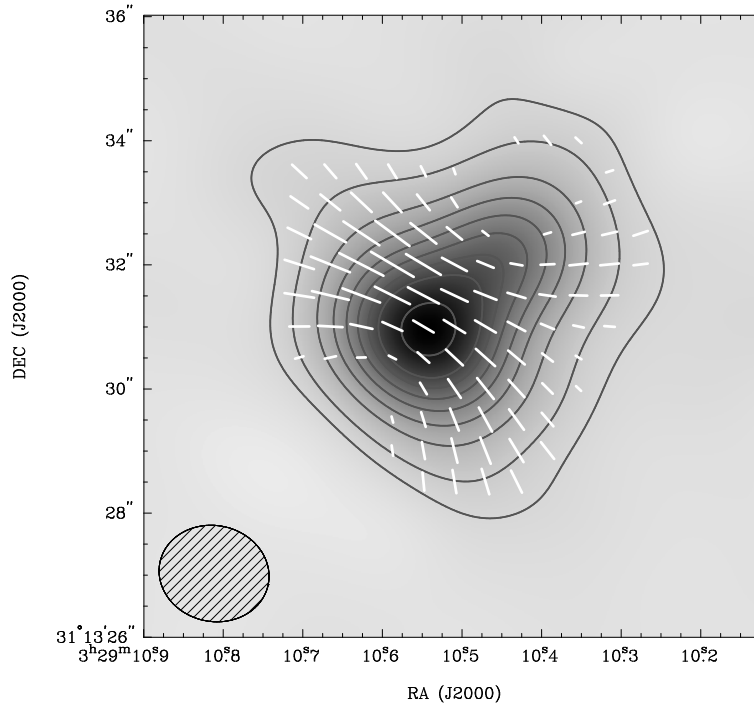


Figure 3. Polarization in the protostar NGC 1333 IRAS 4A, as measured by the SMA polarimeter. Continuum emission is shown in grayscale and contours. The magnetic field direction (orthogonal to the polarization direction) is shown with vectors, their length is proportional to the polarized flux. This observation provided the first clear evidence of an hourglass-shaped magnetic field on the scales expected for isolated star formation.¹⁸

4. SAMPLE SCIENTIFIC RESULTS

The SMA polarimeter was installed on the array in April, 2004 and became available for general use as a facility instrument in November, 2005. The first scientific result from the instrument¹ was the measurement of the 345 GHz linear polarization of the supermassive black hole at the center of our Galaxy, Sagittarius A*. Thanks to the angular resolution and sensitivity of the SMA, the emission from Sgr A* was cleanly separated from the surrounding dust emission and intraday variations in the polarization were detected for the first time. Many subsequent observations have also investigated the magnetic structure in star-forming regions. Fig. 3 is an example¹⁸ of this type of observation in the low-mass protostellar system NGC 1333 IRAS4A. The structure in the field on arcsecond scales matches very well with theoretical predictions of the warping of an initially uniform magnetic field due to the collapse of the magnetized cloud. However, previous observations had lacked the sensitivity and angular resolution to confidently detect this “hourglass” shape.

5. CONCLUSIONS AND FUTURE IMPROVEMENTS

We have presented the 345 GHz polarimeter instrument for the Submillimeter Array. This instrument now provides a fully-supported polarization observing mode for the SMA, used in roughly 10% of observations with the array. Several upgrades to the polarimeter are planned or have been completed since its deployment. As part of a new calibration system, the installation and removal of the wave plates was automated in 2007. Additional wave plates for 230/690 GHz and 240/400 GHz have been added; commissioning of these plates is ongoing. Over the coming year, the SMA will gain a new 340-420 GHz receiver that will provide dual-polarization observations near 345 GHz. This obviates the need for rapid switching of the antenna polarization state, although some polarization modulation is still desirable to prevent errors in the orientation of the derived polarization due to inter-receiver phase drift. The decrease in the switching overhead and the instantaneous measurement of all

four polarized cross correlations will improve the sensitivity by a factor of more than $\sqrt{5}$ for this band, greatly increasing the number of sources accessible to the array.

ACKNOWLEDGMENTS

We are grateful to the staff of the SMA and the SAO submillimeter receiver lab for their assistance during the design and testing of the polarimeter. We thank Ken Young for his tireless work adapting the correlator software to accommodate this new observing mode. We also thank the director of the SMA, Ray Blundell, and the past director, Jim Moran, for their support for this instrument.

REFERENCES

1. D. P. Marrone, J. M. Moran, J.-H. Zhao, and R. Rao, "Interferometric Measurements of Variable 340 GHz Linear Polarization in Sagittarius A*," *ApJ* **640**, pp. 308–318, Mar. 2006.
2. R. J. Sault, J. P. Hamaker, and J. D. Bregman, "Understanding radio polarimetry. II. Instrumental calibration of an interferometer array," *A&AS* **117**, pp. 149–159, May 1996.
3. J. S. Greaves, W. S. Holland, T. Jenness, A. Chrysostomou, D. S. Berry, A. G. Murray, M. Tamura, E. I. Robson, P. A. R. Ade, R. Nartallo, J. A. Stevens, M. Momose, J.-I. Morino, G. Moriarty-Schieven, F. Ganaway, and C. V. Haynes, "A submillimetre imaging polarimeter at the James Clerk Maxwell Telescope," *MNRAS* **340**, pp. 353–361, Apr. 2003.
4. H. Li, C. D. Dowell, L. Kirby, G. Novak, and J. E. Vaillancourt, "Design and initial performance of sharp, a polarimeter for the shar-ii camera at the caltech submillimeter observatory," *Appl. Opt.* **47**(3), pp. 422–430, 2008.
5. B. R. Johnson, M. E. Abroe, P. Ade, J. Bock, J. Borrill, J. S. Collins, P. Ferreira, S. Hanany, A. H. Jaffe, T. Jones, A. T. Lee, L. Levinson, T. Matsumura, B. Rabii, T. Renbarger, P. L. Richards, G. F. Smoot, R. Stompor, H. T. Tran, and C. D. Winant, "MAXIPOL: a balloon-borne experiment for measuring the polarization anisotropy of the cosmic microwave background radiation," *New Astronomy Review* **47**, pp. 1067–1075, Dec. 2003.
6. P. Oxley, P. A. Ade, C. Baccigalupi, P. deBernardis, H.-M. Cho, M. J. Devlin, S. Hanany, B. R. Johnson, T. Jones, A. T. Lee, T. Matsumura, A. D. Miller, M. Milligan, T. Renbarger, H. G. Spieler, R. Stompor, G. S. Tucker, and M. Zaldarriaga, "The EBEX experiment," in *Infrared Spaceborne Remote Sensing XII. Edited by Strojnik, Marija. Proceedings of the SPIE, Volume 5543, pp. 320-331 (2004).*, M. Strojnik, ed., *Presented at the Society of Photo-Optical Instrumentation Engineers (SPIE) Conference 5543*, pp. 320–331, Nov. 2004.
7. R. Rao, *Measurement of magnetic fields from linear polarization of dust emission*. PhD thesis, University of Illinois, 1999.
8. R. L. Akeson, J. E. Carlstrom, J. A. Phillips, and D. P. Woody, "Millimeter Interferometric Polarization Imaging of the Young Stellar Object NGC 1333/IRAS 4A," *ApJ* **456**, pp. L45+, Jan. 1996.
9. S. Pancharatnam, "Achromatic Combinations of Birefringent Plates; II, An Achromatic Quarter-Wave Plate," *Proc. Indian Acad. Sci.* **A41**, p. 137, 1955.
10. A. M. Title, "Improvement of birefringent filters. 2: Achromatic waveplates," *Appl. Opt.* **14**, pp. 229–237, Jan. 1975.
11. S. Hanany, J. Hubmayr, B. R. Johnson, T. Matsumura, P. Oxley, and M. Thibodeau, "Millimeter-wave achromatic half-wave plate," *Appl. Opt.* **44**, pp. 4666–4670, Aug. 2005.
12. J.-B. Masson and G. Gallot, "Terahertz Achromatic Quarter-Wave Plate," *Optics Letters* **31**(2), pp. 265–267, 2006.
13. K. M. Menten, G. J. Melnick, T. G. Phillips, and D. A. Neufeld, "A new submillimeter water maser transition at 325 GHz," *ApJ* **363**, pp. L27–L31, Nov. 1990.
14. J. W. Lamb, "Miscellaneous data on materials for millimeter and submillimeter optics," *Int. J. IR and Millimeter Waves* **17**, pp. 1997–2034, Dec. 1996.

15. J. R. Birch, G. J. Simonis, M. N. Afsar, R. N. Clarke, J. M. Dutta, H. M. Frost, A. Hadni, W. F. Hall, R. Heidinger, and W. W. Ho, "Intercomparison of measurement techniques for the determination of the dielectric properties of solids at near millimeter wavelengths," *IEEE Transactions on Microwave Theory Techniques* **42**, pp. 956–965, June 1994.
16. M. N. Afsar, "Precision millimeter-wave dielectric measurements of birefringent crystalline sapphire and ceramic alumina," *IEEE Transactions on Instrumentation Measurement* **36**, pp. 554–559, June 1987.
17. D. P. Marrone, *Submillimeter Properties of Sagittarius A**. PhD thesis, Harvard University, 2006.
18. J. M. Girart, R. Rao, and D. P. Marrone, "Magnetic Fields in the Formation of Sun-Like Stars," *Science* **313**, pp. 812–814, Aug. 2006.